Bound-free intersubband absorption in *p*-type doped semiconductor quantum wells

M. Tadić* and Z. Ikonić
Faculty of Electrical Engineering, University of Belgrade, Bulevar Revolucije 73, 11000 Belgrade, Yugoslavia
(Received 4 April 1995)

A procedure is proposed for calculating the light absorption due to transitions from bound- to free-hole states in semiconductor quantum wells. The continuum spectrum is described via the scattering states approach. In calculating the transition-matrix elements, account is taken of the position dependence of Luttinger parameters. Example calculations in $GaAs/Al_xGa_{1-x}As$ quantum wells indicate that bound-free absorption may dominate over bound-bound absorption in the wavelength range of interest for practical applications. It is also found that the position of the absorption peak is essentially influenced by states with nonzero transverse wave vector, due to the high nonparabolicity of the valence-band dispersion. This implies that energies of virtual states in the continuum cannot be simply deduced from the absorption profile. Transitions from the heavy-hole ground state to continuum give the principal contribution to absorption, the light-hole contribution being an order of magnitude lower. Calculated results show very good agreement with experimental measurements [K. M. S. V. Bandara *et al.*, Phys. Rev. B **48**, 7999 (1993)].

I. INTRODUCTION

Intersubband optical transitions between the conduction-band states, or between the valence-band states in semiconductor quantum wells, have recently attracted considerable attention, mostly in view of perspective application of these structures for infrared detection, or in nonlinear optical devices. The intersubband absorption in *n*-type doped quantum wells based on direct-band-gap semiconductors may occur only for light polarized perpendicularly to the quantum-well plane. In *p*-type doped wells this restriction is lifted, and the in-plane polarized (i.e., normally incident) light is also absorbed, which is considered their significant technical advantage over *n*-type doped wells. This was first achieved with a multiple $GaAs/Al_xGa_{1-x}As$ quantum-well structure infrared detector.[1] Single-quantum-well detectors have also recently been proposed,[2] with somewhat different characteristics from those of multiple-quantum-well detectors, but with a similar spectral range of responsivity. Unlike their *n*-type doped counterparts,[3–5] *p*-type doped structures do not require waveguide or grating couplers, and absorb light of any polarization or angle of incidence. However, their responsivities as infrared detectors are still an order of magnitude behind those obtained in *n*-type doped structures. The responsivity vs bias dependence in the two types of structures are also quite different, the linear dependence found in the *p*-type doped structure of Ref. 2 indicating that bound-free transitions make the largest contribution to absorption and infrared detection. The photoconductive gain in *p*-type doped structures is not as large as in *n*-type doped ones, but this results in reduced noise, enabling the detectivity in excess of 10^{10} cm $\sqrt{\text{Hz}}$/W.

Although normal-incidence absorption is also possible in *n*-type doped quantum-well structures made of indirect-band-gap semiconductors[6–10] or narrow direct-band-gap semiconductors,[11] the *p*-type doped wells are no less important for applications, as demonstrated by practically realized detectors based upon them.[1,2] The intersubband absorption in *p*-type doped structures was theoretically considered by Chang and James[12] for $GaAs/Al_xGa_{1-x}As$ quantum wells. A structure based on $GaSb/Al_xGa_{1-x}Sb$ has also been proposed[13] in order to increase the absorption due to the reduced heavy-hole effective mass (heavy-hole states make the dominant contribution to absorption). Another interesting system is the one based on $In_{0.53}Ga_{0.47}As/InP$,[14] offering shorter wavelengths ($\sim 2.7\ \mu$m) due to a large valence-band discontinuity of the interface. The theory of Chang and James has also been applied to strained structures based on $In_xGa_{1-x}As/In_xAl_{1-x}As$,[15] $In_xGa_{1-x}As/Al_xGa_{1-x}As$,[16] and $In_xGa_{1-x}As/InP$,[17] where modified bound-state ordering leads to different spectral characteristics than in lattice-matched cases. Almost all theoretical considerations deal explicitly with the topmost four valence bands (i.e., with heavy and light holes), which is justified due to the fact that the conduction band and the hole split-off band are usually remote enough. Indeed, the $GaAs/Al_xGa_{1-x}As$ system has also been considered within the 8×8 Hamiltonian model,[18] with results very similar to those obtained by the 4×4 Hamiltonian model, not surprising in view of a rather large band gap ($E_g \approx 1.4$ eV) and the spin-orbit splitting ($\Delta = 0.34$ eV). Most considerations were devoted to transitions between bound states, although bound-free transitions are no less important. A simplified treatment of bound-free transitions, based upon the concept of resonant states in the continuum, and therefore similar to the case of bound-bound transitions, has been given in Ref. 16. In another paper on this topic[18] the method was not discussed in any detail. Very recently, upon the completion of this work, a report appeared[19] on the calculation of bound-free absorption in superlattices. Periodic boundary conditions for envelope wave functions were

0163-1829/95/52(11)/8266(10)/$06.00

used, as appropriate, making this approach essentially different from the one employed in our work.

In this paper we present a procedure for calculating the bound-free absorption in p-type doped quantum wells. For simplicity, but with essentially no loss of accuracy, we work within the axial approximation in the block-diagonalized Hamiltonian for the electronic structure calculation, and use appropriate results for the transition-matrix elements.[20] Free-hole states are described in terms of scattering states (after Ref. 21 but adapted to the more complex case of the valence band), and bound states are calculated as described in Ref. 22. The self-consistency effects are neglected here, although the method allows for straightforward modifications to take them into account, where necessary. In Sec. II we describe the calculation of free-hole states (the case of bound states is extensively covered in the literature, and needs not be repeated here), and in Sec. III the appropriate expression for the absorption is derived. Numerical calculations on a specific example of $GaAs/Al_xGa_{1-x}As$ quantum-well structure, grown along the [001] direction, are presented and discussed in Sec. IV.

II. FREE-HOLE STATES WAVE FUNCTIONS

We start from the Luttinger-Kohn Hamiltonian[23] with the four topmost Γ_8 valence bands of the zinc-blende crystal, written in the representation whose basis states are the projections of the total angular momentum $J=\frac{3}{2}$:

$$\hat{H}=\begin{bmatrix} P+Q & -S & R & 0 \\ -S^\dagger & P-Q & 0 & R \\ R^\dagger & 0 & P-Q & S \\ 0 & R^\dagger & S^\dagger & P+Q \end{bmatrix}, \tag{1}$$

with

$$P=\frac{\hbar^2}{2m_0}\gamma_1(k_t^2+k_z^2)\ , \quad Q=\frac{\hbar^2}{2m_0}\gamma_2(k_t^2-2k_z^2)\ ,$$

$$R=-\frac{\hbar^2}{2m_0}\gamma_2\sqrt{3}(k_x^2-k_y^2)+i\frac{\hbar^2}{2m_0}\gamma_3 2\sqrt{3}k_xk_y\ ,$$

$$S=\frac{\hbar^2}{2m_0}\gamma_3 2\sqrt{3}(k_x-ik_y)k_z\ ,$$

where m_0 is the free-electron mass, $\gamma_{1,2,3}$ are Luttinger parameters describing the influence of higher and lower bands not included in the basis, $k_{x,y,z}$ are the wave-vector components along the corresponding crystal axes, and $k_t=\sqrt{k_x^2+k_y^2}$ is the transverse (in-plane) wave number. The energy is measured from the valence-band top downwards. With the structure composition, and hence the potential, modulated along the z axis (the [001] growth direction for the quantum well is assumed here), k_z in Eq. (1) is replaced by the operator $-i\partial/\partial z$, and the terms of the form $w(z)k_z^2$ by their Hermitian operator are equivalent $(-i\partial/\partial z)w(z)(-i\partial/\partial z)$, where $w(z)$ is a corresponding combination of Luttinger parameters which are material, and hence position dependent. Furthermore, the potential $V(z)$, representing the valence-band edge, is added to the diagonal terms in Eq. (1). The basis functions of the Hamiltonian (1) are

$$|\tfrac{3}{2},\tfrac{3}{2}\rangle=-\frac{1}{\sqrt{2}}|(X+iY)\uparrow\rangle\ ,$$

$$|\tfrac{3}{2},\tfrac{1}{2}\rangle=-\frac{1}{\sqrt{6}}|(X+iY)\downarrow\rangle+\sqrt{\tfrac{2}{3}}|Z\uparrow\rangle\ ,$$

$$|\tfrac{3}{2},-\tfrac{1}{2}\rangle=\frac{1}{\sqrt{6}}|(X-iY)\uparrow\rangle+\sqrt{\tfrac{2}{3}}|Z\downarrow\rangle\ ,$$

$$|\tfrac{3}{2},-\tfrac{3}{2}\rangle=\frac{1}{\sqrt{2}}|(X-iY)\downarrow\rangle\ ,$$

where X, Y, and Z denote the crystal unit-cell periodic parts of Bloch wave functions, with the same symmetry as atomic x, y, and z functions, and arrows denote the spin-up ($\uparrow$) or spin-down ($\downarrow$) functions. This is the conventional choice of basis, although some others are also occasionally used.[24]

Hamiltonian (1) may be simplified by applying a unitary transform, and using at the same time the axial approximation (neglecting the difference of γ_2 and γ_3 in the off-diagonal term R) to obtain

$$\hat{H}_{b\text{-}d}=\begin{bmatrix} H_U & 0 \\ 0 & H_L \end{bmatrix}=\begin{bmatrix} P+Q+V(z) & \tilde{R} & 0 & 0 \\ \tilde{R}^\dagger & P-Q+V(z) & 0 & 0 \\ 0 & 0 & P-Q+V(z) & \tilde{R} \\ 0 & 0 & \tilde{R}^\dagger & P+Q+V(z) \end{bmatrix}, \tag{2}$$

with two uncoupled 2×2 blocks H_U and H_L, where

$$\tilde{R}=|R|-i|S|\ , \quad |R|=\frac{\hbar^2}{2m_0}\frac{\sqrt{3}}{2}(\gamma_2+\gamma_3)k_t^2\ ,$$

$$|S|=\frac{\hbar^2}{2m_0}2\sqrt{3}\gamma_3k_tk_z\ .$$

The state vector corresponding to Hamiltonian (2) is of length 4, i.e., $F=[F_1F_2F_3F_4]^T$, where F_{1-4} are the envelope functions. In the general case of an asymmetric structure the upper and lower blocks of (2) deliver quantized states with mutually unequal energies, and the corresponding state vectors $[F_1F_2]^T$ and $[F_3F_4]^T$ are fully independent of each other. However, in the symmetric

structures that we deal with in this paper, the two blocks of (2) will give two degenerate sets of states (Kramers degeneracy), and their state vectors, although different, are related by symmetry transformations. Due to the continuity of the full wave function and current conservation, it follows that the envelope function state vectors

$$\begin{bmatrix} F_1 \\ F_2 \end{bmatrix} \tag{3}$$

and

$$\begin{bmatrix} (\gamma_1-2\gamma_2)d/dz & \sqrt{3}k_t\gamma_3 \\ -\sqrt{3}k_t\gamma_3 & (\gamma_1+2\gamma_2)d/dz \end{bmatrix} \begin{bmatrix} F_1 \\ F_2 \end{bmatrix} \tag{4}$$

for the upper block, and analogous expressions for the lower block, are continuous across the structure composition discontinuities, i.e., the well/barrier interfaces.[25]

Using Eq. (2) and the continuity of (3) and (4), the bound-state eigenenergies in a quantum well are calculated by the transfer-matrix method algorithm, described in Ref. 22. Here we discuss in more detail the calculations of free-state wave functions. We should first note that in the free part of energy spectrum $\hat{H}_{b\text{-}d}F=EF$ has solutions for any energy, and furthermore there is a degeneracy present. In calculation of the optical properties, or hole density, the objective is to find a complete set of orthonormalized states, so that all states are counted just once, and none is omitted. A suitable set of wave functions for this purpose are scattering states. In the field of semiconductor microstructures these were used by Kriman, Kluksdahl, and Ferry for the conduction-band states within the effective-mass approximation. However, the conduction-band states are comparatively simple, because at any energy there is a single pair of bulk states, either both evanescent or both propagating, and continuum states in a microstructure may equally easily be counted by imposing distant box boundary conditions.[26,27] On the other hand, the valence-band states in a microstructure generally involve two pairs of coupled bulk states, and, depending on energy, both pairs may be evanescent or both propagating, or one of each kind may occur. The second possibility, which is realized in a large part of the free spectrum, makes it quite difficult to apply the box boundary conditions, and scattering states are a natural choice.

Consider a one-dimensional (1D) localized binding scattering potential, hereafter called the well, present in the bulk, which is, sufficiently away from the well, unperturbed, having (asymptotically, at least) flat bands. A scattering state in this system would comprise an incident wave and the set of transmitted and reflected waves it generates, all of them being plane waves in the 1D case. A hole incident wave from the left, say, is written as $[F_1F_2]^T$ multiplied by a normalization constant $1/\sqrt{2\pi}$, where the envelope wave-function state vector $[F_1F_2]^T$ is the bulk solution of Eq. (2), subject to the condition $|F_1(-\infty)|^2+|F_2(-\infty)|^2=1$. The phase factor which describes the plane wave with the wave vector $\mathbf{k}=(k_t,k)$ is contained in the envelope functions $F_{1,2}$, their amplitudes themselves being calculated for this particular value of $\mathbf{k}$. With a total of four wave-vector branches, i.e., solutions of hole dispersion relation in bulk,[28] there may be up to four independent scattering states for every block with the same energy, their incident wave components being given as described. To make proper scattering states one should first classify the bulk states, with their corresponding k vectors, according to the following criterium. Bulk states with real k (propagating) should be tested for the current they carry, and if it is found positive the state is classified as forward; otherwise it is backward. We should note that current direction is not uniquely related to the sign of k, and the current evaluation is necessary for proper classification. If k is complex, however, such a (evanescent) state carries no current, and is forward if $\mathrm{Im}(k)>0$ (i.e., decays to the right), and backward if $\mathrm{Im}(k)<0$. Since states appear in $\pm k$ pairs,[28] there will be an equal number of each type. In a proper scattering state of the structure, the incident wave can be only a current-carrying state incoming to the well (i.e., bringing the current inside). Thus the current-carrying forward states on the left-hand side, and current-carrying backward states on the right-hand side, are the incident waves. These generate outgoing

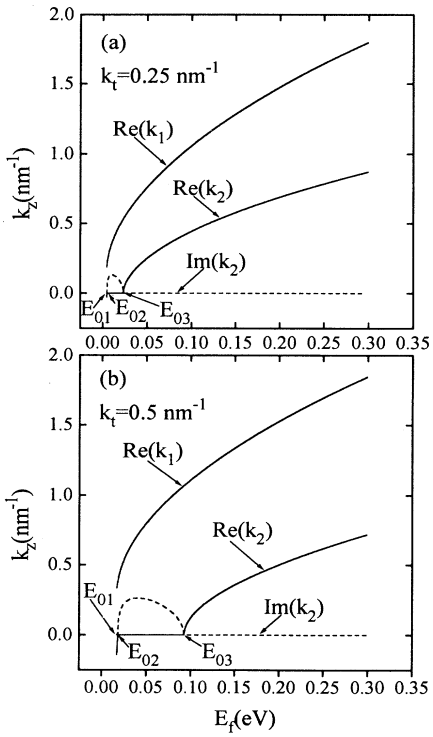

FIG. 1. The z component of the free-hole-state wave vector vs the energy dependence, calculated for the transverse wave-vector component $k_t=0.25$ nm^{-1} (a), $k_t=0.5$ nm^{-1} (b), k_1 and k_2 corresponding to heavy-hole-like and light-hole-like states, respectively. The real parts of $k_{1,2}$ are represented by solid lines, and imaginary parts by broken lines (only k_2 may have the imaginary component, while k_1 is real throughout the free spectrum). The energy where k_1 becomes real is denoted as E_{01}, while E_{02} and E_{03} denotes energies between which only k_2 is imaginary.

(transmitted and reflected) states, which either carry current or their wave functions decay outwards from the well. Thus backward states on the left-hand side and forward states on the right-hand side constitute the transmitted and reflected waves in scattering states.

According to this, three parts of the free-energy spectrum may be distinguished for any nonzero value of the transverse wave number k_t. Just above the range of low energies, where all four k vectors are complex and thus allow for the existence of bound states, lies the first part of free-energy spectrum [$E_{01} < E < E_{02}$ in Figs. 1(a) and 1(b)] where all k vectors are real. Consequently, four scattering states, two left- and two right-incident, exist in this part. In the second part, $E_{02} < E < E_{03}$ in Figs. 1(a) and 1(b), two k vectors are real and the other two complex (the former are heavy-hole-like, the latter are light-hole-like), so just two scattering states exist here. We should note that the signs of k_2 and the signs of the current for propagating states are related in the opposite manner for $E < E_{02}$ and $E > E_{02}$. As the transverse wave number k_t increases, the width of this part also increases, but at $k_t = 0$ it does not exist, due to heavy- and light-hole degeneracy at the valence-band top. Above this second part, once all the wave vectors have become real, lies the third part ($E > E_{03}$) of the free spectrum which, as far as intersubband transitions are concerned, may be taken to extend to infinity. All this is illustrated in Figs. 1(a) and 1(b) for two values of k_t, on the example of a $Al_{0.3}Ga_{0.7}As$ bulk, the characteristic energies being denoted by E_{01}, E_{02}, and E_{03}. With the incident wave amplitude given as above, all the others (transmitted and reflected waves) are found by analytical or numerical solution of the Schrödinger equation once the potential and other structure parameters are specified. This is actually done by constructing the transfer T matrix of the system, as an intermediate step. This relates the amplitudes of the waves on the right-hand side of the well (c_r) to those on the left-hand side (c_l), i.e.,

$$\begin{bmatrix} c_{r1} \\ c_{r2} \\ c_{r\bar{1}} \\ c_{r\bar{2}} \end{bmatrix} = [T] \begin{bmatrix} c_{l1} \\ c_{l2} \\ c_{l\bar{1}} \\ c_{l\bar{2}} \end{bmatrix} , \tag{5}$$

where, e.g., $\bar{1}$, the second subscript to the amplitude, denotes that this corresponds to $k = -k_1$ (since states appear in pairs, $k_3 = -k_1$ and $k_4 = -k_2$). The transfer matrix may be found, element by element, by shooting each single wave, evanescent or propagating (one at a time), with unity amplitude toward the well from the left-hand side. The first column of T, for example, simply equals the amplitudes of plane waves on the right-hand side of the well when excited by $e^{ik_1 z}$ on the left. To calculate these amplitudes, therefore, we solve the system of differential equations

$$(\gamma_1 - 2\gamma_2)\frac{d^2F_1}{dz^2} = \left\{(\gamma_1+\gamma_2)k_t^2 + \frac{2m_0}{\hbar^2}[V(z)-E]\right\}F_1 + \frac{\sqrt{3}}{2}(\gamma_2+\gamma_3)k_t^2 F_2 - 2\sqrt{3}\gamma_3 k_t \frac{dF_2}{dz} , \tag{6}$$

$$(\gamma_1 + 2\gamma_2)\frac{d^2F_2}{dz^2} = \left\{(\gamma_1-\gamma_2)k_t^2 + \frac{2m_0}{\hbar^2}[V(z)-E]\right\}F_2 + \frac{\sqrt{3}}{2}(\gamma_2+\gamma_3)k_t^2 F_1 + 2\sqrt{3}\gamma_3 k_t \frac{dF_1}{dz} , \tag{7}$$

with the initial conditions on the left-hand side,

$$\begin{bmatrix} F_{l1} \\ F_{l2} \end{bmatrix} = \begin{bmatrix} A \\ B \end{bmatrix} e^{ik_1 z_{0l}} , \tag{8}$$

where $[A\ B]^T$ (with $|A|^2 + |B|^2 = 1$) is the bulk-state vector corresponding to the wave vector k_1, and z_{0l} is the initial coordinate (in the bulk, where bands are flat). The integration proceeds up to a point z_0 on the right-hand side, and also in the bulk where the potential is again flat. In the special case of a rectangular quantum well $2d$ wide, and with the self-consistency effects neglected, i.e., with $V(z) = 0$ for $|z| > d$, it is enough (and best for the numerical error minimization) to set $z_{0l} = -d$ and $z_0 = d$. In the inner region (the well), the differential equations (6) and (7) are integrated numerically, as in Ref. 22, observing the continuity of vectors (3) and (4). While the special case of a rectangular well also allows for an analytic solution, numerical integration was actually used here in order to enable the inclusion of self-consistency effects at a latter stage. Having obtained the envelope function amplitudes $F_{1,2}$, together with their derivatives on the right-hand side (at z_0), one now has to represent them as a linear combination of plane waves which are bulk solutions in this region. This is done by solving the system of linear equations[22]

$$\begin{bmatrix} A_{r1}e^{ik_1z_0} & A_{r2}e^{ik_2z_0} & A_{r\bar{1}}e^{-ik_1z_0} & A_{r\bar{2}}e^{-ik_2z_0} \\ B_{r1}e^{ik_1z_0} & B_{r2}e^{ik_2z_0} & B_{r\bar{1}}e^{-ik_1z_0} & B_{r\bar{2}}e^{-ik_2z_0} \\ ik_1A_{r1}e^{ik_1z_0} & ik_2A_{r2}e^{ik_2z_0} & -ik_1A_{r\bar{1}}e^{-ik_1z_0} & -ik_2A_{r\bar{2}}e^{-ik_2z_0} \\ ik_1B_{r1}e^{ik_1z_0} & ik_2B_{r2}e^{ik_2z_0} & -ik_1B_{r\bar{1}}e^{-ik_1z_0} & -ik_2B_{r\bar{2}}e^{-ik_2z_0} \end{bmatrix} \begin{bmatrix} c_{r1}^{(i)} \\ c_{r2}^{(i)} \\ c_{r\bar{1}}^{(i)} \\ c_{r\bar{2}}^{(i)} \end{bmatrix} = \begin{bmatrix} F_{r1} \\ F_{r2} \\ F'_{r1} \\ F'_{r2} \end{bmatrix} . \tag{9}$$

The above procedure is repeated four times, the superscript i in Eq. (9) taking values from the set $(1, \bar{1}, 2, \bar{2})$, and the obtained solutions for the amplitudes c make the corresponding columns of the transfer matrix.

The next step is to recast the transfer matrix into the scattering (S) matrix, that relates the incoming to outgoing waves in the system

$$\begin{bmatrix} c_{r1} \\ c_{r2} \\ c_{l\bar{1}} \\ c_{l\bar{2}} \end{bmatrix} = [S] \begin{bmatrix} c_{l1} \\ c_{l2} \\ c_{r\bar{1}} \\ c_{r\bar{2}} \end{bmatrix} , \tag{10}$$

where obviously the forward waves on the left and backward waves on the right are incoming states, and the rest are outgoing ones.

The transfer and scattering matrices (both are 4×4) are related by

$$S_{11}=T_{11}-T_{12}T_{22}^{-1}T_{21} , \quad S_{12}=T_{12}T_{22}^{-1} , \quad S_{21}=-T_{22}^{-1}T_{21} , \quad S_{22}=T_{22}^{-1} , \tag{11}$$

where T_{ij} and S_{ij} ($i=1,2$; $j=1,2$) are their 2×2 blocks, i.e.,

$$[T]=\left[\begin{array}{c|c} T_{11} & T_{12} \\ \hline T_{21} & T_{22} \end{array}\right] , \quad [S]=\left[\begin{array}{c|c} S_{11} & S_{12} \\ \hline S_{21} & S_{22} \end{array}\right] . \tag{12}$$

The individual elements of the S matrix are in fact the amplitudes of various transmitted and reflected waves excited by the corresponding unity amplitude incident waves, and this essentially completes the construction of the scattering states set. With at most four incident waves possible, the same is the number of scattering states, and they are given by

$$F_{Ul}^{(i)}(z)=\begin{cases} \dfrac{1}{\sqrt{2\pi}} \begin{bmatrix} A_i \\ B_i \end{bmatrix} e^{ik_i z}+s(3,i) \begin{bmatrix} A_{\bar{1}} \\ B_{\bar{1}} \end{bmatrix} e^{-ik_1 z}+s(4,i) \begin{bmatrix} A_{\bar{2}} \\ B_{\bar{2}} \end{bmatrix} e^{-ik_2 z} , & z<-d , \quad i=1,2 \\ s(1,i) \begin{bmatrix} A_1 \\ B_1 \end{bmatrix} e^{ik_1 z}+s(2,i) \begin{bmatrix} A_2 \\ B_2 \end{bmatrix} e^{ik_2 z} , & z>d , \quad i=1,2 , \end{cases} \tag{13}$$

$$F_{Ur}^{(i-2)}(z)=\begin{cases} s(3,i) \begin{bmatrix} A_{\bar{1}} \\ B_{\bar{1}} \end{bmatrix} e^{-ik_1 z}+s(4,i) \begin{bmatrix} A_{\bar{2}} \\ B_{\bar{2}} \end{bmatrix} e^{-ik_2 z} , & z<-d , \quad i=3,4 \\ \dfrac{1}{\sqrt{2\pi}} \begin{bmatrix} A_{\bar{i}} \\ B_{\bar{i}} \end{bmatrix} e^{-ik_i z}+s(1,i) \begin{bmatrix} A_1 \\ B_1 \end{bmatrix} e^{ik_1 z}+s(2,i) \begin{bmatrix} A_2 \\ B_2 \end{bmatrix} e^{ik_2 z} , & z>d , \quad i=3,4 , \end{cases} \tag{14}$$

where the subscripts l and r denote the states incident from the left or from the right. In the case of just two bulk states being propagating [i.e., in the energy range between E_{02} and E_{03} in Figs. 1(a) and 1(b)] the scattering states in the structure are also given by Eqs. (13) and (14), but with $i=1$ and 3 only. The scattering states' wave functions inside the well are found by numerical integration, as described above, with the initial conditions contained in Eqs. (13) and (14). The procedure for finding the lower block scattering states is completely analogous.

Finally, we may note that the special case of a rectangular well allows for direct (not via the T matrix) and analytical evaluation of the S-matrix elements. However, with each scattering state demanding the solutions of four systems of (8×8) linear equations, this analytic solution is too cumbersome to be reproduced here.

III. THE ABSORPTION

We start from the expression giving the absorption coefficient within the dipole approximation,[29]

$$\alpha(\omega)=\frac{\pi q^2}{n\epsilon_0 c\omega\Omega}\sum_{i,f}|\langle f|\mathbf{a}\mathbf{v}|i\rangle|^2\delta(E_f-E_i-\hbar\omega) \times[f_n(E_i)-f_n(E_f)] , \tag{15}$$

where q is the electron charge, n the refractive index, ϵ_0 the dielectric permittivity of vacuum, c the speed of light, Ω the volume of the structure, and $\mathbf{a}$ the unit vector of light polarization. The initial and final hole state energies are E_i and E_f, $\hbar\omega$ is the photon energy, and f_n is the Fermi-Dirac distribution function for holes.

Expression (15) is applicable to n-dimensional electron or hole gas ($n=0$, 1, 2, and 3). In the two-dimensional case (confinement along one direction) the physically meaningful quantity is the fractional absorption per well,[29] and the absorption coefficient of a sample with a number of quantum wells may then be straightforwardly deduced.

The transition-matrix element in Eq. (15) should include the full (detailed) wave functions of the two states involved, while only the envelope functions are normally

obtained in the electronic structure calculation. An appropriate expression for the transition-matrix element that requires only the envelope functions has been previously derived[12] for the case of position-independent Luttinger γ parameters and within the 4×4 (not block-diagonalized) Hamiltonian. It was subsequently used for the absorption calculations in conventional and strained structures as well.[15,16] We have recently given a simplified derivation for the transition-matrix elements that allows for the position-dependent γ parameters, and which uses the wave functions of the block-diagonalized 2×2 Hamiltonian,[20] and these results are employed here. We may note that the position-dependent Luttinger parameters were taken in the intersubband absorption calculations in Ref. 17, but the final results were not correct, because the unitary transform that block diagonalizes the basic Hamiltonian does not block diagonalize the interaction Hamiltonian.[19,20] The transition-matrix element for inter-valence-subband transitions can be written as

$$\overline{|M_{\rm eff}|^2}=\overline{|M_{UU}|^2}+\overline{|M_{UL}|^2}+\overline{|M_{LU}|^2}+\overline{|M_{LL}|^2}\ , \tag{16}$$

where the overbar simply denotes that averaging over the angles between the light polarization vector and the in-plane wave vector of hole states has been performed in each term in Eq. (16). The first and fourth terms $\overline{|M_{UU}|^2}$ and $\overline{|M_{LL}|^2}$ describe transitions between states of the upper and lower block of the Hamiltonian (2), respectively, and the second and third terms $\overline{|M_{UL}|^2}$ and $\overline{|M_{LU}|^2}$ to transitions between states of the lower block, the first (second) subscript denoting the block to which the final (initial) state belongs. The four terms are given by

$$\begin{aligned}\overline{|M_{UU}|^2}=&\tfrac{1}{2}|2(\gamma_{11}^{(+)}+\gamma_{22}^{(-)}+\sqrt{3}\overline{\gamma}_{12}+\sqrt{3}\overline{\gamma}_{21})k_t\\&-i\sqrt{3}(\Pi_{12}-\Pi_{21})|^2a_t^2\\&+|\Pi_{11}^{(-)}+\Pi_{22}^{(+)}-i2\sqrt{3}k_t(\overline{\gamma}_{12}-\overline{\gamma}_{21})|^2a_z^2\ ,\end{aligned} \tag{17}$$

$$\overline{|M_{LU}|^2}=\tfrac{3}{2}|\Pi_{31}-\Pi_{42}+i2k_t(\overline{\gamma}_{31}-\overline{\gamma}_{42})|^2a_t^2\ , \tag{18}$$

$$\overline{|M_{UL}|^2}=\tfrac{3}{2}|\Pi_{13}-\Pi_{24}-i2k_t(\overline{\gamma}_{13}-\overline{\gamma}_{24})|^2a_t^2\ , \tag{19}$$

$$\begin{aligned}\overline{|M_{LL}|^2}=&\tfrac{1}{2}|2(\gamma_{44}^{+}+\gamma_{33}^{(-)}+\sqrt{3}\overline{\gamma}_{34}+\sqrt{3}\overline{\gamma}_{43})k_t\\&-i\sqrt{3}(\Pi_{34}-\Pi_{43})|^2a_t^2\\&+|\Pi_{44}^{(-)}+\Pi_{33}^{(+)}-i2\sqrt{3}k_t(\overline{\gamma}_{34}-\overline{\gamma}_{43})|^2a_z^2\ ,\end{aligned} \tag{20}$$

where a_t and a_z denote the in-plane and perpendicular components of the light polarization unit vector (e.g., for normal incidence $a_t=1$ and $a_z=0$), while Π and γ with appropriate subscripts denote the weighted momentum matrix elements and weighted overlap integrals, respectively, both being calculated with the envelope functions only:

$$\Pi_{ji}=\langle F_j^f|\Pi|F_i^i\rangle\ , \tag{21}$$

$$\gamma_{ji}=\langle F_j^f|\gamma|F_i^i\rangle\ . \tag{22}$$

Here the superscripts i and f denote the initial and final states, and subscripts denote the corresponding envelope function component of the state vector. More specifically, the matrix elements of operators

$$\gamma^{(\pm)}=\gamma_1(z)\pm\gamma_2(z)\ , \tag{23}$$

$$\overline{\gamma}=\frac{\gamma_2(z)+\gamma_3(z)}{2}\ , \tag{24}$$

$$\Pi^{(\pm)}=(\gamma_1\pm2\gamma_2)k_z+k_z(\gamma_1\pm2\gamma_2)\ , \tag{25}$$

$$\Pi=\overline{\gamma}k_z+k_z\overline{\gamma}\ , \tag{26}$$

where $k_z=-i\partial/\partial z$, should be calculated.

The absorption due to bound-bound transitions is given by

$$\begin{aligned}A(\hbar\omega)=&\frac{q^2\hbar^3}{8n\epsilon_0cm_0^2\hbar\omega}\\&\times\int_0^\infty k_t\,dk_t\sum_{i,f}\overline{|M_{\rm eff}|^2}[f_n(E_i)-f_n(E_f)]\\&\times\frac{\Gamma/2\pi}{(E_f-E_i-\hbar\omega)^2+\Gamma^2/4}\ ,\end{aligned} \tag{27}$$

where the δ function of Eq. (15) is replaced by a Lorentzian with the full width parameter Γ, to model various broadening mechanisms.

The absorption on bound-free transitions is given by a similar expression in which the summation over discrete final states turns into the integral over the final-state wave vector k_z (it is important here that final states should be properly normalized).[21] However, due to the nonparabolicity of the dispersion, it is convenient to change from integration over k_z to integration over the final-state energy E_f, to obtain

$$A(\hbar\omega)=\frac{q^2\hbar^3}{8n\epsilon_0cm_0^2\hbar\omega}\int_0^\infty k_t\,dk_t\sum_i\int_{E_{01}}^\infty M_{\rm eff}^g[f_n(E_i)-f_n(E_f)]\frac{\Gamma/2\pi}{(E_f-E_i-\hbar\omega)^2+\Gamma^2/4}dE_f\ . \tag{28}$$

Here E_{01} denotes the energy where the wave vector k_1 becomes real (as depicted in Fig. 1). The quantity $M_{\rm eff}^g$ in (26) is a sum of the form

$$M_{\rm eff}^g=\begin{cases}2\overline{|M_{{\rm eff},1}|^2}\dfrac{dk_1}{dE_f}+2\overline{|M_{{\rm eff},2}|^2}\dfrac{dk_2}{dE_f}\ , & E_{01}<E_f<E_{02}\ ,\ E_f>E_{03}\\ 2\overline{|M_{{\rm eff},1}|^2}\dfrac{dk_1}{dE_f}\ , & E_{02}<E_f<E_{03}\ ,\end{cases} \tag{29}$$

where the individual terms are the transition-matrix elements squared and multiplied by the energy derivative of the real wave number characterizing the left-incident final hole state, and the factor 2 accounts for the fact that left- and right-incident states make equal contributions, so it suffices to take just one of them in calculation. Equation (29) thus gives the density-of-states weighted transition-matrix element squared, hence the superscript g.

IV. NUMERICAL RESULTS AND DISCUSSION

Numerical calculations, according to the framework described above, were done for a 4-nm-wide GaAs quantum well embedded in $Al_{0.3}Ga_{0.7}As$ bulk. Values of Luttinger parameters in GaAs (AlAs) are $\gamma_1=6.85$ (3.45), $\gamma_2=2.10$ (0.68), and $\gamma_3=2.90$ (1.29), and linear interpolation was used for the alloy. We take that the valence-band discontinuity at the $GaAs/Al_xGa_{1-x}As$ interface amounts to 150 meV, the same as in Ref. 2. The refraction index in the bulk, $Al_{0.3}Ga_{0.7}As$ equals $n=3.6-0.7x=3.39$,[30] and this value is assumed for the whole structure, since the major part of it is the bulk (and it is not very different from 3.6 in the GaAs well). Hole density per unit well surface is taken to be 1×10^{12} cm^{-2}, as in Refs. 13 and 16. The Lorentzian width is taken as $\Gamma=13.16$ meV, corresponding to the (intraband) relaxation time $\tau_{in}=0.1$ ps.[16,24]

There are three hole bound states in this quantum well, HH1, LH1, and HH2 in order of increasing energy. Among the three possible bound-bound transitions, the LH1→HH2 one is the weakest, its matrix element being considerably lower than for the other two transitions (HH1→HH2 and HH1→LH1). The absorption spectrum for the two dominant transitions (the case of normal incidence) is given in Fig. 2, showing a very good agreement with the results of Ref. 16. Maximum absorption occurs at low photon energies, where the phonon-scattering-assisted absorption may even prevail over the direct intersubband absorption, and the first peak at 28.5 may not then be really visible[31] (it is out of the most interesting spectral range anyway). A considerably lower peak due to the HH1→HH2 transition is positioned at 100 meV, and should be experimentally detectable. We may also note that these results are obtained with the position dependence of Luttinger parameters taken into account, but even if this was discarded small differences in the percent range could be found. A larger difference of Luttinger parameters in the two materials would be necessary to produce any real effect in bound-bound transitions.

Concerning the spectral range of principal interest for

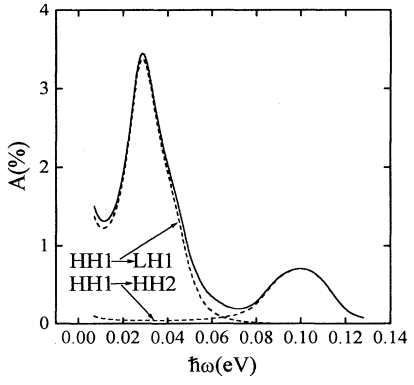

FIG. 2. The bound-bound absorption vs photon energy dependence, calculated for a $2d=4$-nm-wide GaAs well in $Al_{0.3}Ga_{0.7}As$ bulk, with a hole sheet density of 10^{12} cm^{-2}, at $T=77$ K. The large absorption at low energies occurs on HH1→LH1, while $HH_1\rightarrow HH_2$ contributes in the range considered to be more interesting for applications. The case of normal-light incidence is considered only.

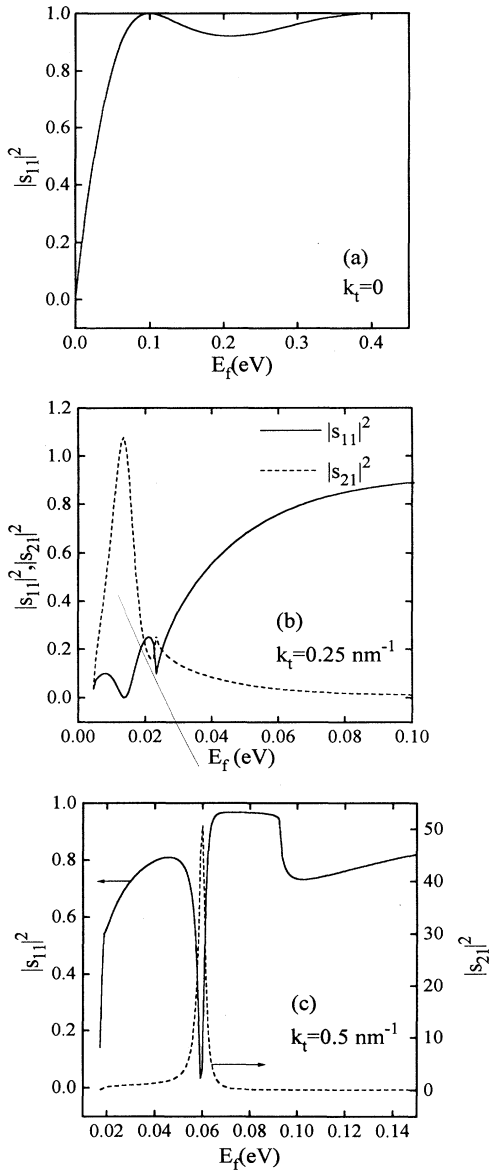

FIG. 3. The free-hole-state energy dependence of the S-matrix elements squared, $|s_{11}|^2$ and $|s_{21}|^2$ for the transverse wave number $k_t=0$ (a) ($|s_{21}|^2\equiv0$ in this case), $k_t=0.25$ nm^{-1} (b), and $k_t=0.5$ nm^{-1} (c).

applications (8–14 μm), the main contribution to absorption in this quantum well stems from bound-free transitions. To discuss them in some more detail, in Figs. 3(a)–3(c) we give the S-matrix elements s_{11} and s_{21} squared, as they depend on the final-state energy for different values of the transverse wave vector k_t: $k_t=0$ [Fig. 3(a); heavy and light holes are decoupled and $|s_{21}|^2\equiv 0$ in this case], $k_t=0.25$ nm^{-1} [Fig. 3(b)], and $k_t=0.5$ nm^{-1} [Fig. 3(c)]. $|s_{11}|^2$ and $|s_{21}|^2$ are the probabilities for the left-incident heavy-hole state to come out as heavy- and light-hole states, respectively, on the right-hand side (due to state mixing for $k_t\neq 0$, the state characters should be understood as predominantly heavy- and light-hole-like). For $k_t=0$, absent the state mixing, $|s_{11}|^2$ depends on energy in the classical textbook manner, never exceeding unity. The other coefficient $|s_{21}|^2$, however, may exceed unity for $k_t\neq 0$ at low enough energies [Figs. 3(b) and 3(c)] which is not unusual in view of the fact that state 2 is evanescent, carrying no current. For $k_t=0.5$ nm^{-1}, $|s_{11}|^2$ is about constant as energy varies, except for a dip at $E=60$ meV, where $|s_{21}|^2$ has a sharp peak.

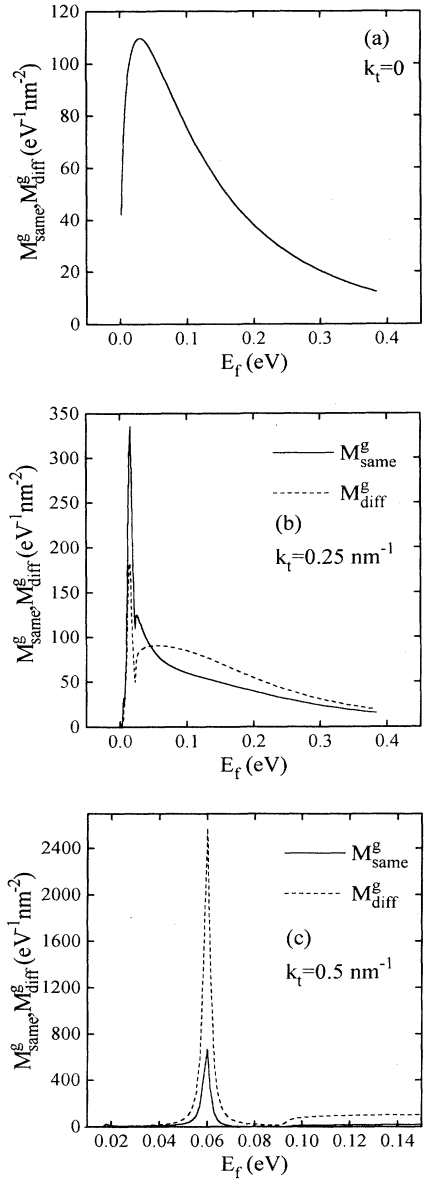

FIG. 4. The dependence of the two components of g-matrix elements, M^g_{same} and M^g_{diff} (defined in the text) on free-state energy, calculated for $k_t=0$ (a) ($M^g_{same}\equiv M^g_{diff}$ in this case), $k_t=0.25$ nm^{-1} (b), and $k_t=0.5$ nm^{-1} (c).

Considering the case of normal light incidence, the two components of the density-of-states-weighted effective matrix element $M^g_{same}=M^g_{UU}+M^g_{LL}$ and $M^g_{diff}=M^g_{UL}+M^g_{LU}$ for transitions between the ground heavy-hole state (HH1) and the continuum, are given in Figs. 4(a)–4(c), as they depend on final-state energy for different k_t values. For $k_t=0$, due to the fact that only Π terms in (17)–(20) contribute, and due to symmetries of the wave functions and the S-matrix elements, the two components are equal [Fig. 4(a)]. For not too large k_t values, γ terms in (17)–(20) are less important than Π terms, and thus M^g_{same} and M^g_{diff} do not differ much, but M^g_{same} is somewhat larger [Fig. 4(b)]. As k_t increases further, however, the ratio M^g_{diff}/M^g_{same} exceeds unity: at $k_t=0.5$ nm^{-1}, M^g_{diff} is about four times greater than

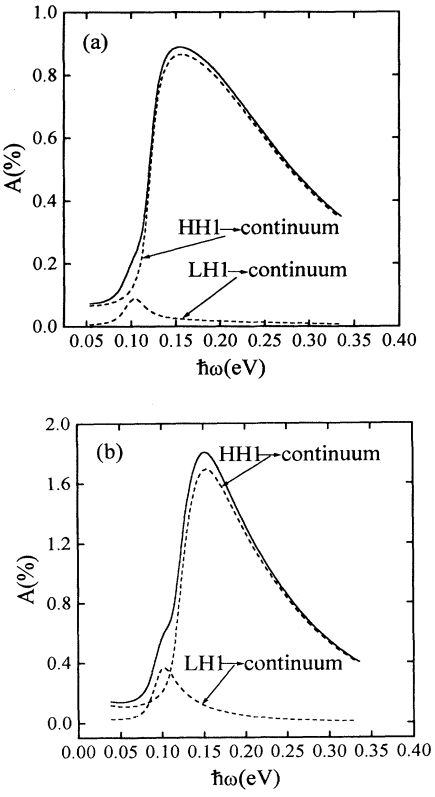

FIG. 5. The bound-free-absorption profile in the case of normal-light incidence (a) and parallel incidence (b) for the structure with the same parameters as in Fig. 2. The largest absorption occurs on HH1→continuum transitions, and a much smaller one on LH1→continuum ones. The two separate contributions are given by broken lines, and the full absorption by the solid line. The HH2→continuum transitions are negligible, and are not displayed.

M^g_{same} [Fig. 4(c)]. Therefore, for larger k_t values the block-flip transitions are more probable than block-conserving transitions between hole states. This is in complete contrast to the case of conduction-band states, where the spin-flip transitions are only slightly allowed, and are negligible under most circumstances. Certainly, although very large values of transition-matrix elements are obtainable, their contribution to absorption may still be limited, which is controlled by the difference of distribution functions for the states involved. It is also interesting to note that the positions of matrix element peak values cannot be simply deduced from the energy structure itself (energies of bound states and resonances in continuum), even at $k_t=0$. At the intermediate k_t value of 0.25 nm^{-1}, for instance, the matrix elements have rather smooth peaks at low energies, where the transmission coefficient $|s_{21}|^2$ reaches a maximum [Fig. 4(b)]. For larger k_t, like $k_t=0.5$ nm^{-1}, the transition-matrix elements may have very sharp peaks, the result of a large amplitude of the slowly varying evanescent component of the wave function and rapidly changing density of states for energies close to E_{03} [Fig. 4(c)].

All lines given in Figs. 4(b) and 4(c) have something in common. In the energy range below E_{02} the matrix elements are small, but show sharp peaks between E_{02} and E_{03} (Fig. 1) followed by a slow decrease for $E>E_{03}$ (where all the k vectors are real). The energy range most useful for overall absorption is that where propagating and evanescent states in the bulk coexist. To obtain larger responsivities of infrared detectors, one should design the structure to favor a fast variation of the transition-matrix elements in this energy range. This could be achieved by tailoring the well shape (by grading composition); however, this constitutes a problem of its own, and will not be considered here.

The full bound-free absorption is mostly due to HH1→continuum transitions, as depicted in Fig. 5, for normally incident [Fig. 5(a)] and parallely incident [Fig. 5(b)] light. Transitions from LH1 to continuum make a comparatively small contribution, the peak being at lower energies than the main absorption peak. Finally, the absorption on HH2→continuum transitions is very small, mostly due to the high energy of the HH2 state which is close to the top of the well. Note also that the full absorption profile is more smeared than that for bound-bound transitions, where multiple peaks may be observed (Fig. 2). We find the absorption peak to be positioned at 154.5 meV, which differs substantially from the transition energy from the HH1 bound state to the heavy-hole quasibound (resonant) state in continuum calculated as in Ref. 16. The absorption amounts to 0.89% (peak value), with the full width at half maximum equal to 6.3 μm. A slow decrease of $|s_{11}|^2$ and $|s_{21}|^2$ for energies higher than E_{03} [Fig. 3(b)] results in asymmetric transition-matrix elements [Fig. 4(b)], which in turn gives a very wide absorption line shape. The positions of the peak absorption and peak value of M^g_{eff} at $k_t=0$ do not coincide (the former being blueshifted), which means that finite k_t states make a very considerable contribution to the full absorption profile. Indeed, the maximum of M^g_{eff} shifts toward higher energies as k_t increases, due to the combined influence of density of states and evanescent wavefunction amplitude, as discussed above, and so do contributions of these states to the absorption profile.

Our results agree very well with the experimentally measured absorption line shape in quantum-well-based infrared detector structures by Bandara, Levine, and Kuo[2] where a single peak of the responsivity spectrum has been observed (according to the simple theory of Andrews and Miller,[32] it corresponds to the peak absorption). The relative error between the measured[2] and calculated results amount to ~10%, the latter being redshifted by 0.8 μm from the measured peak absorption at 7.2 μm.

However, there are at least four reasons that this disagreement might have been expected. The experimentally realized structure had very limited width and a special type of doping, with the equilibrium Fermi level determined by acceptor density in its contacts. Furthermore, the spectral responsivity was measured under bias, not under asymptotically flat-band conditions, as were assumed in this work. Finally, as noted in Ref. 2, there is a significant charge redistribution and self-consistency effects appear. Although the estimated self-consistent potential is about 15 meV,[2] not as large as is typical in n-type doped structures, it still may shift the absorption peak by roughly this amount. The proximity of the spin split-off band is an additional factor that may effect absorption to some extent, especially for photon energies close to Δ.

Further improvement and generalization of the model we used would include the effects of self-consistency (due to filling of both bound- and free-hole states), in a way similar to that employed for n-type doped wells.[27] Furthermore, the spin-split-off band states might also be included for better accuracy, e.g., using the Hamiltonian given in Ref. 33.

V. CONCLUSION

A method for calculation of intersubband absorption on bound-free transitions in p-type doped semiconductor quantum wells was presented. Numerical calculations were performed for a $GaAs/Al_xGa_{1-x}As$-based structure. In the specific example studied we found a fractional absorption of 0.89% (peak value) at a wavelength of 8 μm, which makes the structure perspective for infrared detection. The calculated results agree very well with experimental measurements, with errors of about 10%. Smaller values of absorption were found on bound-bound heavy-hole transitions as well. We have shown that a simple model that considers only bound states and resonant states in the continuum cannot give an accurate description of the absorption profile, because all relevant quantities on which the absorption depends vary strongly with the transverse wave number.

*Electronic address: tadic@kiklop.etf.bg.ac.yu

[1]B. F. Levine *et al.*, Appl. Phys. Lett. **59**, 1864 (1991).
[2]K. M. S. V. Bandara, B. F. Levine, and J. M. Kuo, Phys. Rev. B **48**, 7999 (1993).
[3]L. S. Yu *et al.*, J. Appl. Phys. **72**, 2105 (1992).
[4]K. M. S. V. Bandara *et al.*, J. Appl. Phys. **74**, 1826 (1993).
[5]B. F. Levine, Semicond. Sci. Technol. **8**, S400 (1993).
[6]C.-L. Yang, D.-S. Pan, and R. Somoano, J. Appl. Phys. **65**, 3253 (1989).
[7]E. R. Brown and S. J. Eglash, Phys. Rev. B **41**, 7559 (1990).
[8]H. Xie, J. Katz, and K. L. Wang, J. Appl. Phys. **72**, 3681 (1992).
[9]J. S. Park, R. P. G. Karunasiri, and K. L. Wang, Appl. Phys. Lett. **61**, 681 (1992).
[10]S. K. Chun, D. S. Pan, and K. L. Wang, Appl. Phys. Lett. **62**, 1119 (1993).
[11]R. Q. Yang, J. M. Xu, and M. Sweeny, Phys. Rev. B **50**, 7474 (1994).
[12]Y.-C. Chang and R. B. James, Phys. Rev. B **39**, 12 672 (1989).
[13]H. Xie *et al.*, J. Appl. Phys. **71**, 2844 (1992).
[14]S. D. Gunapala *et al.*, J. Appl. Phys. **72**, 2105 (1992).
[15]H. Xie, J. Katz, and W. I. Wang, Appl. Phys. Lett. **59**, 3601 (1991).
[16]D. Teng, C. Lee, and L. F. Eastman, J. Appl. Phys. **72**, 1539 (1992).
[17]S. A. Stoklitsky *et al.*, Appl. Phys. Lett. **65**, 1706 (1994).
[18]P. Man and D. S. Pan, Appl. Phys. Lett. **61**, 2799 (1992).
[19]L. Tsang and S.-L. Chuang, IEEE J. Quantum Electron. **31**, 20 (1995).
[20]Z. Ikonić, V. Milanović, and M. Tadić, J. Phys. Condens. Matter (to be published).
[21]A. M. Kriman, N. C. Kluksdahl, and D. K. Ferry, Phys. Rev. B **36**, 5953 (1987).
[23]J. M. Luttinger and W. Kohn, Phys. Rev. **97**, 869 (1955); J. M. Luttinger, *ibid.* **102**, 1030 (1956).
[24]G. Jones and E. P. O'Reilly, IEEE J. Quantum Electron. **29**, 1344 (1993).
[25]L. C. Andreani, A. Paquarello, and F. Bassani, Phys. Rev. B **36**, 5887 (1987).
[26]Z. Ikonić, V. Milanović, and D. Tjapkin, Appl. Phys. Lett. **54**, 247 (1989).
[27]M. Tadić, V. Milanović, and Z. Ikonić, Phys. Rev. B **47**, 10 415 (1993).
[28]S. L. Chuang, Phys. Rev. B **43**, 9649 (1991).
[29]U. Bockelmann and G. Bastard, Phys. Rev. B **45**, 1688 (1992).
[30]W. Streifer, D. R. Scifres, and R. D. Burnham, Appl. Opt. **18**, 3457 (1979).
[31]Z. Ikonić *et al.*, Phys. Rev. B **37**, 3097 (1988).
[32]S. R. Andrews and B. A. Miller, J. Appl. Phys. **70**, 993 (1991).
[33]B. A. Foreman, Phys. Rev. B **48**, 4964 (1993).